Sustainable Cities and Society 135 (2025) 107018

Contents lists available at ScienceDirect

Sustainable Cities and Society

journal homepage: www.elsevier.com/locate/scs

The influence of urban morphological changes on pluvial flooding during urban expansion

Yue Zhu [a,*], Paolo Burlando [b], Ye Zhang [c], Dengkai Chi [a], Jing Wang [a], Yeshan Qiu [a], Matteo Bonatesta [b], Wenyue Zou [d], Christian Geiß [e,f], Puay Yok Tan [g], Simone Fatichi [h]

[a] Future Cities Laboratory, Singapore-ETH Centre, Singapore
[b] Institute of Environmental Engineering, ETH Zurich, Switzerland
[c] School of Architecture, Tsinghua University, China
[d] Institute of Earth Surface Dynamics, University of Lausanne, Switzerland
[e] German Remote Sensing Data Center (DFD), German Aerospace Center (DLR), Germany
[f] Department of Geography, University of Bonn, Germany
[g] Department of Architecture, National University of Singapore, Singapore
[h] Department of Civil and Environmental Engineering, National University of Singapore, Singapore

ARTICLE INFO

Keywords:
Urban morphology
Urban expansion
Pluvial flood
Flood resilience

ABSTRACT

Urban expansion alters landscape structure and hydrological processes, heightening pluvial flood risks in cities worldwide. This study integrates multi-temporal urban expansion data with the CAFlood cellular automata model to simulate rainfall events with multiple return periods (i.e., 1-in-10, 1-in-100, and 1-in-200 year return periods) across three different urban environments: Shenzhen (China), suburban Houston (United States), and Lausanne (Switzerland). To quantify how evolving urban morphology drives flood volume, we computed key landscape metrics describing impervious extent (percentage of impervious surface), green space shape complexity (Area-weighted Mean Shape Index), green space aggregation (Aggregation Index), and impervious edge complexity (Landscape Shape Index). Their effects on changes in flood volume were analysed with Generalised Additive Models stratified by levels of pre-expansion impervious cover. The results show that decreasing green space aggregation and impervious edge complexity are consistently significant indicators of increased flood volumes, particularly in areas with low pre-expansion impervious cover (<50 %). However, the influence of these two key morphological indicators decline as impervious coverage increases, with total imperviousness gradually becoming the dominant factor. Sensitivity experiments with synthetic urban fabrics confirm that maintaining compact, well-connected green spaces can limit the increase in flood volume even with when impervious surfaces expand equally. By explicitly linking the morphological changes in urban form to pluvial flood response across diverse climates and urbanisation context, this study moves beyond static approaches and provides actionable insights for planning flood-resilient urban growth.

1. Introduction

1.1. Urban expansion and rising pluvial flood risks

Urban flooding is a growing global challenge driven by climate change and rapid urbanisation (Jian et al., 2020; Rentschler et al., 2023). Climate change is altering precipitation patterns, leading to an increase in the frequency and intensity of extreme rainfall events (Fowler et al., 2021; Moustakis et al., 2021; Tradowsky et al., 2023). Concurrently, cities expand into natural and rural areas, replacing permeable land with impervious surfaces that impede infiltration (Rosenberger et al., 2021) and often encroach on hazard-prone zones (Rentschler et al., 2023), and modify natural drainage systems (Tran et al., 2024). These processes have substantially increased pluvial flood frequency and magnitude worldwide (Muis et al., 2015), underscoring the importance of producing effective and generalisable strategies for flood-resilient urban development.

Urban green spaces are widely recognised as an effective nature-based solution for mitigating pluvial flooding by enhancing infiltration, evapotranspiration, and thus reducing runoff (Li et al., 2020; Su

* Corresponding author at: Future Cities Laboratory, Singapore-ETH Centre, Singapore.
E-mail address: yue.zhu@sec.ethz.ch (Y. Zhu).

https://doi.org/10.1016/j.scs.2025.107018
Received 3 August 2025; Received in revised form 28 October 2025; Accepted 24 November 2025
Available online 25 November 2025

et al., 2024). These benefits have prompted strong advocacy for integrating green infrastructure into urban drainage strategies (Baida et al., 2024; Huang et al., 2020a). More recently, rather than only focusing on the influence of the spatial extent of impervious or pervious surfaces on flooding, efforts have begun to examine how the spatial configuration of green spaces and built-up areas influences flood dynamics (Kim & Park, 2016; Mabrouk et al., 2024; Zhu et al., 2024). Studies show that higher fragmentation and greater shape complexity disrupt green-space continuity, shorten flow paths, and accelerate surface runoff, increasing peak discharge and flood risk (Li, et al., 2023). The connectedness of green spaces also affects flooding by forming multi-scale ecological corridors and infiltration pathways that store rainwater, slow overland flow, and directly influence the size of inundation areas during flood events (Dai & Tan, 2024). Likewise, high edge density of impervious surfaces can fragment and degrade natural drainage networks, causing faster and more concentrated runoff that elevates flood hotspot density (Lin et al., 2023). Building footprints with complex or irregular edges further amplify flood hazards by obstructing and redirecting runoff, constraining drainage paths, and creating backwater effects that elevate local flood volume (Zhu et al., 2024). These findings demonstrate that, even with the same total amount of impervious and pervious areas, the spatial morphology of urban landscapes, such as fragmentation of green space and edge density of impervious surfaces, can affect pluvial flooding (Lin et al., 2023; Zhang et al., 2015).

1.2. The changes in urban morphology and pluvial flooding during urbanisation

However, most existing studies linking urban morphology and pluvial flooding rely on static representations of urban patches, capturing landscape configuration and flood conditions at a single instance in time (Balaian et al., 2024; Lin et al., 2023). This approach can not reflect the inherently dynamic nature of urban expansion, which involves spatio-temporally heterogeneous changes in land surface and the built environment (Fenta et al., 2017). Consequently, studies relying on static representations of urban patches often overlook how the transformation of urban morphology influences the changes in flooding during the process of urbanisation.

Only a limited number of studies have attempted to examine how temporal changes in urban morphology influence floods (Idowu & Zhou, 2023; Mabrouk et al., 2024). Notably, urban growth encompasses not only outward expansion but also densification and redevelopment within existing boundaries, resulting in complex, evolving morphological patterns over time (Broitman & Koomen, 2015; Chakraborty et al., 2022). However, previous studies investigating the influence of temporal urban morphology changes on flooding tend to rely on the simplified typologies of urban growth. For instance, Idowu & Zhou (2023) conducted a correlation analysis employing three broad urban expansion typologies (i.e., infill, leapfrog, or edge expansion), reporting that leapfrog and edge expansion were more associated with high flood risk, whereas infilling shows only a weak association. In contrast, Mabrouk et al. (2024) applied long-term flood-risk mapping based on satellite imagery and GIS analysis, finding that unplanned infill development showed the strongest correlation with flood-vulnerable zones. These seemingly misaligned findings may stem from the broad categories of expansion typologies used in both studies. Given that broad typologies often encompass a wide range of morphological variations, resulting in high internal heterogeneity, categorising urban expansion patterns into a few main types may overlook finer-scale characteristics (Dibble et al., 2019), such as changes in shape complexity and edge configuration. These variations can be further amplified by local context, geographic setting, and planning regimes (Li, et al., 2021; Wang, et al., 2024). As a result, such broad categories of expansion typologies may oversimplify spatial heterogeneity of urban expansion and may lead to inconsistent interpretations about the dynamic interaction between urban form and flooding.

Urbanisation is also a cumulative process that progressively replaces natural land covers, fragments green spaces, and disrupts their spatial connectivity (Li et al., 2019; Wang et al., 2022). This reduces both local ecological functions and landscape-scale capacities for surface runoff regulation (Mitchell & Devisscher, 2022; Xu et al., 2020). In addition, previous studies have shown that the ecological performance of green spaces under urbanisation may exhibit threshold effects, where ecological functions decline sharply once a critical limit is crossed (Alberti & Marzluff, 2004; Ran et al., 2023; Xu et al., 2016). However, there is a lack of thorough investigation into whether similar threshold effects apply to their hydrological functions, particularly in surface runoff regulation. As such, a significant research gap persists in understanding how morphological changes in urban landscapes at different stages of urbanisation influence runoff production and flood risk.

1.3. Research questions and significance

Considering these research gaps, this study investigates how changes in urban morphology influence pluvial flooding, moving beyond previous literature that relied mainly on single-timepoint or broad urban-expansion typologies. Specifically, it focuses on three key questions: (i) Which morphological characteristics of urban landscape (i.e., green spaces and impervious surfaces) most influence changes in pluvial flooding during urbanisation? (ii) Do the effects of these morphological changes vary across different levels of impervious surface coverage? (iii) What are the implications for planning flood-resilient urban expansions? To address these questions, we integrate multi-temporal urban expansion data with the CAFlood cellular automata model to simulate a series of comparable flood scenarios under multiple return-period events (1-in-10, 1-in-100, and 1-in-200 year return periods), ensuring consistent evaluation of flood responses in a variable-controlled manner. We then apply Generalised Additive Models (GAMs) to quantify relationships between evolving landscape metrics and flood volume, allowing detection of nonlinear responses and threshold effects. This combined framework provides a dynamic, indicator-specific, and cross-context assessment of how urban morphology influences potential pluvial flooding. By quantifying how changes in urban form configuration associate with flood dynamics, the study advances understanding beyond static or typology-based analyses and offers actionable guidance for flood-resilient urban planning.

2. Materials and methods

2.1. Study areas and datasets

Three study areas were selected for analysis: (i) Shenzhen, (ii) a suburban area of Houston, and (iii) Lausanne (Fig. 1). These areas were chosen based on the availability of urban expansion datasets and high-resolution DEM data required for pluvial flood simulation, as well as their distinct climatic and terrain conditions, thus aiming to provide a sufficiently broad perspective to allow some general conclusions. Shenzhen, located in the Pearl River Delta of southern China, has a subtropical monsoon climate characterised by hot and humid summers, as well as frequent intense rainstorms and occasional typhoons (Tian et al., 2022). The suburban area of Houston lies in the Gulf Coast region of the United States, with a humid subtropical climate, low elevation, and high exposure to extreme precipitation from tropical storms and sporadic hurricanes (Zhu et al., 2021a). Lausanne, situated on the northern shore of Lake Geneva in Switzerland, has a hilly terrain and a temperate climate with relatively moderate rainfall intensities (Vavassori et al., 2023). Comparing these three distinctive urban areas allows an assessment of whether the identified relationships between urban morphology and pluvial flooding hold across contrasting climatic, topographic, and planning contexts. This strengthens the robustness of the analysis and can potentially provide generalisable insights for translating research outcomes into urban flood management and

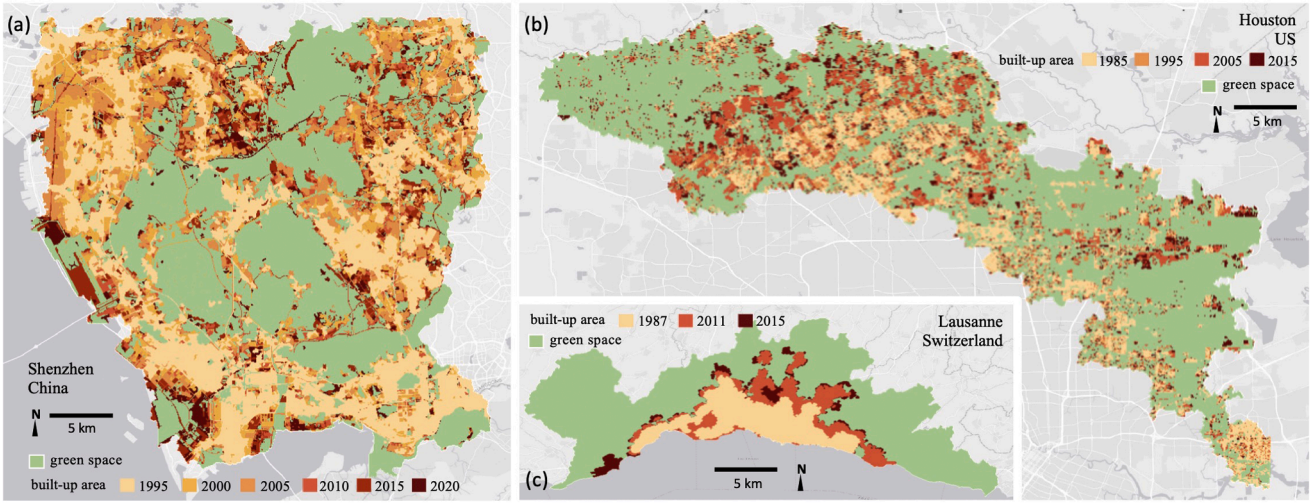

Fig. 1. The datasets of urban expansion in three study areas: (a) the urban expansion of Shenzhen from 1995 to 2020, (b) the expansion of Lausanne from 1987 to 2015, and (c) the expansion in a suburban area in Houston from 1985 to 2015.

land-use planning strategies.

The urban expansion data were collected from multiple sources. The data of Shenzhen was extracted from remote sensing imagery (i.e. Landsat series) with a 5-year interval from 1995 to 2020, with a 10m spatial resolution, using deep-learning-based methods for data augmentation (Zhu et al., 2021b) and multitemporal land cover classification (Zhu et al., 2021c). The urban expansion data of Houston was derived from the dataset of World Settlement Footprint (WSF) 2015 (Marconcini et al., 2020), and is available from 1985 to 2015 with a 10-year interval and a 30m spatial resolution. The urban expansion data of Lausanne was collected from the Atlas of Urban Expansion (Angel et al., 2012), which is an open-source database of satellite imagery. The data is available for three years, 1987, 2011, and 2015, with a 30m spatial resolution. All the three urban expansion datasets were resampled from 30m spatial resolution to 8m resolution using Nearest Neighbour in ArcGIS to match the spatial resolution of flood simulation. Considering that the start and end years differ among these datasets, the analysis focuses on morphological change between subsequent time steps within each city and the corresponding flood response, rather than analysing trends on reconstructed time-series that would require identical temporal intervals. The slightly different time intervals across the three case studies also increase the diversity of real-world urbanisation scenarios represented and strengthen the evaluation of whether the relationships between morphological change and flood response hold under different urban expansion contexts. All urban-form indicators were normalised to enable direct comparison of change magnitudes across the three cities and their different time spans.

2.2. Pluvial flood simulation

The main objective of this study is to quantify how changes in urban landscape morphology influence potential pluvial flood volume, and therefore, the modelling framework was designed to focus on overland flow processes in a controlled and comparable manner across cities. Data of pluvial flood maps were generated using CAFlood (Guidolin et al., 2016), which is a cellular automata model that has been widely employed in studies of urban floods (Huang et al., 2020b; Pallathadka et al., 2022; Rasool et al., 2025; Zhu et al., 2024). The CAFlood model was selected for this study because it provides a highly efficient, physically consistent cellular automata framework well suited for large-scale or data-limited urban applications (Guidolin et al., 2016). Unlike conventional hydrodynamic models that require detailed knowledge of the drainage system, CAFlood enables consistent, scenario-based comparisons of flood response under controlled rainfall and land-use conditions. Other widely used urban drainage models such as SWMM (Gironás et al., 2010) and MIKE URBAN (DHI, 2013) are primarily designed for detailed sewer and pipe-network hydraulics, thus requiring extensive sewage system data (rarely available) and often do not consider spatial configuration of vegetation, making them less suitable for isolating landscape-morphology effects on overland flow and for large-scale scenario testing. Other advanced urban flood models as tRIBS-OFM offer more rigorous process representation (J. Kim et al., 2012), but at the expense of very large computational times.

CAFlood has been validated in previous research through benchmarking against the industry-standard methods, presenting a strong agreement for simulation in both natural terrain and urban areas (Guidolin et al., 2016; Wang et al., 2018). It should be noted that because CAFlood does not account for underground drainage networks, this is treated implicitly by modifying the infiltration rate of impervious surface, which leads to a simplified representation of the complex interactions between underground and surface flows. Nevertheless, CAFlood provides an optimal combination of spatially heterogeneous infiltration representation and computational scalability, as proven in the relevant literature.

One of the key inputs for flood simulation is DEM data. The DEM data of Shenzhen is collected from TanDEM-X with 12-meter spatial resolution (Zink et al., 2017), the DEM data of Houston is from the 3D Elevation Program (3DEP) with 10m spatial resolution (United States Geological Survey, 2021), and the DEM data of Lausanne is from SwissALTI3D with 2m spatial resolution (Wiederkehr & Möri, 2013). For pluvial flood simulations, the DEM data for all three study areas were resampled to an 8m spatial resolution to avoid introducing discrepancies in the simulation approach.

For each available urban land cover map across the three study areas, three rainfall events of varying intensity were simulated, representing 30-minute rainfall with return periods of 1-in-10-year, 1-in-100-year, and 1-in-200-year, respectively, with the corresponding rainfall intensities listed in Table 1. The rainfall intensity values were derived from the Intensity-Duration-Frequency (IDF) curves specific to each study area, collected from official sources released by national or regional agencies, including the Geotechnical Engineering Office of Hong Kong SAR (GEO, 2023), the US National Weather Service (2025), and the Federal Office of Meteorology and Climatology in Switzerland (MeteoSwiss, 2022). As included in Appendix A, the three IDF curves reveal distinct climatic features. The flood simulation for Shenzhen adopted the IDF curves from the adjacent city of Hong Kong, as the two

Table 1
Simulation setup for pluvial flooding in the three study areas. Each area is simulated under three different rainfall scenarios (i.e., 1-in-10-year, 1-in-100-year, and 1-in-200-year return periods), using spatially heterogeneous infiltration rates corresponding to the impervious cover extent of each year.

		Shenzhen, China	Houston, US	Lausanne, Switzerland
Rainfall intensity (30min duration)	1-in-10-year	150 mm/h	60 mm/h	27 mm/h
	1-in-100-year	200 mm/h	88 mm/h	42 mm/h
	1-in-200-year	220 mm/h	98 mm/h	52 mm/h
Infiltration rate	Impervious surface	30 mm/h (30% drainage efficiency)	16 mm/h (30% drainage efficiency)	23 mm/h (100% drainage efficiency)
	Pervious surface	50 mm/h	50 mm/h	50 mm/h

cities share very similar rainfall patterns and are often considered part of the Greater Bay Area, a region characterised by generally similar climatic conditions in many previous studies (Qiang et al., 2020; Tan et al., 2023). Overall, the three IDF curves capture substantial variability in rainfall intensity across climatic regions, thereby enhancing the generalisability of the findings on potential pluvial flood occurrence. Additionally, the slope tolerance (a minimum slope threshold applied to avoid the zero-slope instability) was set to 0.1 % for all simulations, following the configuration previously validated as optimal for urban pluvial flood simulation (Guidolin et al., 2016).

A binary infiltration mask was generated for each land cover map: urban areas were classified as impervious surfaces, while vegetation and water bodies were treated as pervious surfaces. This setup allows each flood simulation to capture the influence of urban morphological changes at different stages of expansion in a simplified but effective way. The infiltration rate for pervious surfaces was set at 50mm/h, corresponding to the typical infiltration capacity of moist loam soil with dense vegetation as suggested in the SWMM manual (Rossman, 2015). Although heterogeneous underground drainage networks can influence how surface runoff is removed, incorporating them, even when data is available, would complicate the study of urban-form effects because drainage capacity vary within each city, and it would introduce city-specific confounding effects that reduce the comparability of cross-city analyses. Instead, CAFlood allows to mimic the efficiency of the urban drainage network, by applying a spatially homogeneous infiltration rate on impervious surfaces to represent the overall effect of the drainage system. The infiltration rates for impervious surfaces were defined to represent drainage capacity, with full capacity corresponding to the ability to fully rainfall intensity of a 5-year return period event, which is commonly regarded as the design target for urban drainage systems in city centres (Butler et al., 2018). To ensure that the effective infiltration of impervious surfaces remains below that of pervious surfaces, impervious surfaces were assigned a drainage efficiency of 30 % for Shenzhen (30 mm/h) and Houston (16 mm/h), and 100 % for Lausanne (23 mm/h).

In total, 36 rainfall events with varying urban landscape morphology were simulated. After generating pluvial floodwater depth maps, the pluvial floodwater volume within each grid cell was calculated based on the floodwater depth D_j and inundation area A_j at each location, using the following formula: $V_{total} = \sum_{j=1}^{n} (A_j \times D_j)$. The change in flood volume between two time steps, t_1 and t_2, was then computed as: $\Delta flood\ volume = V_{total}^{t2} - V_{total}^{t1}$.

2.3. Morphological indicators of urban landscape changes

To characterise the morphological changes of green spaces and impervious surfaces during urbanisation, we employed landscape metrics for each time instance of the land cover maps for all the study areas. The landscape metrics adopted in this study include Percentage of Landscape (PLAND), Landscape Shape Index (LSI), Area-weighted Mean Shape Index (AWMSI), and Aggregation Index (AI). Based on these indicators, we derived several measures to capture morphological changes in urban green spaces and impervious surfaces between consecutive time steps. Specifically, "ΔAWMSI green space" reflects changes in the average shape complexity of green areas, "ΔAI green space" represents the variation in the aggregation of green space, and "ΔLSI impervious surfaces" indicates changes in the edge complexity of impervious surfaces between two spatial maps at specific different points in time. Additionally, "ΔPLAND impervious ratio" was computed to capture changes in total impervious surface coverage over time. The definitions and formulas for each morphological indicator are provided in Table 2. It should be noted that variations in building height and density were not included, as they are not dominant drivers of floodwater distribution, and consistent time-series data of building height were also unavailable. The possible indirect influence of building morphology on rainfall distribution by modifying surface roughness and wind patterns is a complex secondary effect (Torelló-Sentelles et al., 2025; Yang et al., 2024) and goes beyond the scope of this study. The analysis therefore focused on surface urban form under spatially homogeneous rainfall.

2.4. Methods for correlation analysis

To facilitate the correlation analysis, the dependent variables (i.e., urban morphological indicators) and independent variables (i.e., potential pluvial flooding metrics) were sampled at neighbourhood scale using grids. To assess the robustness of the correlation findings to spatial resolution, a sensitivity test was conducted using sampling grids of different size (i.e., 400 m, 800 m, 1200 m) based on Spearman correlations. The results suggest that the directional relationships between the predictor variables and the target variable remain consistent across grids, and larger grid sizes (e.g., 1000 m and 1200 m) tend to yield stronger correlations. Therefore, the 1km grid was finally preferred as it achieves the optimal balance between correlation strength and sufficient number of grid cells compared with other tested grid sizes. The full sensitivity to grid size resolution is reported in Figure B1 (Appendix B). Using the 1 km grids, for each city, urban morphological indicators were computed for each sampling unit, and total flood volume for different return periods were also calculated for each grid cell (Figure B2, Appendix B).

To mitigate multi-colinearlity in correaltion analysis, highly correlated indicators were subsequently removed using Spearman correlation, Variance Inflation Factor (VIF), and tolerance checks. Specifically, we first conducted a Spearman correlation analysis to ensure that no pairs of indicators exhibited high pairwise correlation, all correlation coefficients were below 0.75 across the three study areas (Figure B1, Appendix B). Subsequently, we performed VIF and tolerance checks to assess multicollinearity, confirming that all indicators had VIF values below 3 and tolerance values above 0.4 (Table B1, Appendix B).

GAMs were deployed to model the relationship between changes in urban landscape morphology and changes in pluvial flooding. GAMs are widely used in correlation analysis due to their ability to capture complex, nonlinear relationships between predictors and the response variable (Gomez-Rubio, 2018), which has been increasingly adopted in urban data analysis (Mitchell & Devisscher, 2022; Ravindra et al., 2019). Before training each GAM, the data was normalised using a scaling method that preserves zero values and normalises using the interquartile range (IQR) without centring the data. The scaling method is as follows:

$$x_i' = \frac{x_i}{IQR},\ IQR = Q_3 - Q_i$$

where Q_1 and Q_3 are the first and third quartiles of the indicator value. This scaling method was selected to fit the task of modelling changes in

Table 2
Definitions and equations of morphological indicators of urban landscape changes.

Indicators	Definition	Equation
Percentage of landscape (PLAND) impervious surfaces	The percentage of the total landscape occupied by impervious surface.	$PLAND_{impervious} = \left(\frac{Area\ of\ impervious\ surface}{Total\ area\ of\ the\ sampling\ unit}\right) \times 100$
Landscape Shape Index (LSI) impervious surfaces	LSI measures how complex or irregular the shapes of land patches are. For instance, simple shapes have low LSI, whereas twisty and stretched-out edges tend to have high LSI.	$LSI_{impervious} = \frac{0.25 \times Total\ edge\ length\ of\ impervious\ srufaces}{\sqrt{Total\ area\ of\ the\ sampling\ unit}}$
Area-weighed Mean Shape Index (AWMSI) green space	AWMSI measures the average shape complexity of land patches, but assigns more importance to larger patches. For instance, if the large patches are highly irregular and twisted in shape, AWMSI is high.	$AWMSI_{green} = \sum_{i=1}^{n}\left(\frac{P_{green}}{2\sqrt{\pi A_{green}}} \times \frac{A_{green}}{A_{total}}\right)$ where P_{green} is perimeter of green patch, A_{green} is its area
Aggregation Index (AI) green space	Aggregation index of green space describes how aggregated or clumped green patches are. For instance, AI is high when patches are clustered and form larger areas, and low when they are dispersed and fragmented.	$AI_{green} = \left(\frac{g_{green}}{max\ g_{green}}\right) \times 100$ where $g_{green}$is the number of like adjacencies between pixels of green patches, $max\ g_{green}$ is the maximum number of like adjacencies between pixels of green patches, based on the single-count method.
Δ LSI impervious surfaces	The difference of LSI impervious surfaces between consecutive time steps of land cover maps.	$\Delta\ LSI_{impervious} = LSI^{t_2}_{impervious} - LSI^{t_1}_{impervious}$ where $LSI^{t_1}_{impervious}$ is the value of LSI impervious surfaces at time t_1, and $LSI^{t_2}_{impervious}$ is the value of LSI impervious surfaces at time t_2.
Δ AI green space	The difference of aggregation Index green space between consecutive time steps of land cover maps.	$\Delta\ AI_{green} = AI^{t_2}_{green} - AI^{t_1}_{green}$ where $AI^{t_1}_{green}$ is the value of AI green space at time t_1, and $AI^{t_2}_{green}$ is the value of AI green space at time t_2.
Δ AWMSI green space	The difference of AWMSI green space between consecutive time steps of land cover maps.	$\Delta\ AWMSI_{green} = AWMSI^{t_2}_{green} - AWMSI^{t_1}_{green}$ where $AWMSI^{t_1}_{green}$ is the value of AWMSI green space at time t_1, and $AWMSI^{t_2}_{green}$ is the value of AWMSI green space at time t_2.
ΔPLAND impervious ratio	The ratio of the percentage of impervious surface between consecutive time steps of land cover maps.	$r\Delta PLAND_{impervious} = \left(\frac{PLAND^{t_2}_{impervious} - PLAND^{t_1}_{impervious}}{PLAND^{t_1}_{impervious}}\right)$

urban morphological indicators and flood volume, as it retains both negative and positive values, which are essential for interpreting directional changes over time. By scaling with the IQR without centring, it handles skewed data and reduces the influence of outliers, which can improve both the interpretability and robustness of GAM estimates.

For each rainfall return period and study area, separate GAMs were trained using both the full dataset and four stratified subsets defined by the percentage of pre-expansion urban coverage: (a) less than 25 %; (b) between 25 % and 50 %; (c) between 50 % and 75 %; and (d) greater than 75 %. The percentage of pre-expansion urban coverage reflects the extent to which land within each sampling unit had already been converted from natural to impervious surfaces before subsequent urban expansion. In the process of training each GAM, the dataset was split into training and testing sets, with a split ratio of 80 % training and 20 % testing. Model fitting was performed on the training set, specifically, we employed a 5-fold cross-validation strategy to fine-tune model parameters, including the number of splines, smoothing parameters, and maximum iteration settings. After identifying the best GAM parameter for each flooding event, we assessed model performance and robustness on the testing dataset, using the metrics of R^2 and adjusted R^2.

To facilitate the interpretation of the marginal impact of indicators in GAMs, Partial Dependence Plots (PDP) were generated to show the average effect of each indicator on the predicted outcome, holding other indicators constant (Goldstein et al., 2013), which can highlight the importance of the indicators of urban morphological changes in relation to flood volume changes. Moreover, PDP plots were computed with 95 % confidence intervals to quantify and visualise model uncertainty.

After identifying key morphological indicators, a sensitivity analysis with synthetic urban fabrics was conducted within the flood simulation environment to compare the impact of modified morphological characteristics of the urban landscape on changes in pluvial flooding in varying urban expansion scenarios. This synthetic experiment employed a 1 km^2 urban area in Shenzhen with a rainfall event of a 1-in-100-year return period as the baseline pre-expansion scenario. Building on this baseline, we constructed a series of comparable urban expansion scenarios that share the same total increase in impervious surface but differ in morphological characteristics along a gradient of key indicator values. These scenarios represent the transition from low-density to medium-density development typical of rapidly urbanising areas. By using this controlled set of scenarios, the experiment disentangled the influence of urban form from total impervious coverage on pluvial flood response.

3. Results

3.1. Temporal trends of urban expansion and pluvial flood in the three urban areas

Before analysing correlations, we performed a statistical analysis of

urban landscape morphological indicators for each available year and the simulated extent of potential pluvial flooding (Fig. 2), to inspect the similarities and differences in the overall temporal trends across the three study areas.

In Shenzhen (Fig. 2a), the mean "PLAND impervious surfaces" increased substantially from 1995 to 2020, indicating rapid urban expansion, particularly before 2005. During the same period, mean values of "AWMSI green space" and "LSI impervious surfaces" also rose before 2005, but then plateaued or even slightly decreased afterwards. In contrast, the mean "AI green space" declined consistently, reflecting increasing fragmentation and reduced spatial connectivity of green infrastructure. These morphological changes corresponded to a marked rise in the simulated total flood volume across all rainfall return periods.

In Lausanne (Fig. 2b), most landscape morphological metrics (PLAND, LSI, and AWMSI) showed steady increases over time, while "AI green space" slightly decreased over the three analysed periods. Although total urban flood volume increased substantially, flood volume per unit impervious area remained relatively stable across all return periods.

For the suburban area in Houston (Fig. 2c), "PLAND impervious surface" increased sharply since 1995, accompanied by significant declines in "AI green space". However, changes in "AWMSI green space" were less pronounced than in Lausanne, and "LSI impervious surfaces" even declined after remaining relatively stable prior to 2005. In terms of flooding, total flood volume rose sharply, but flood volume per unit impervious area slightly decreased, showing a distinct trend compared to the other two cities.

Overall, some similar patterns across the three cities can be observed, including an increase in total impervious surfaces accompanied by reduced green-space aggregation and higher total flood volume, yet nuanced variations emerge. Specifically, in Shenzhen, rapid expansion under a humid subtropical monsoon climate and low-lying coastal terrain likely contribute to the steep increase in flood volume. In Lausanne, steady urban growth on sloping terrain with relatively minor loss of green-space aggregation, together with lower rainfall intensity and long-standing green-space planning, may explain the more moderate increase in total flood volume. In Houston, flat areas with a humid subtropical climate prone to heavy storms and a substantial loss of green-space aggregation likely drive the sharp rise in total flood volume. These statistics also highlight that both urban landscape morphology and flood volume exhibit diverse temporal patterns during the process of urban expansion. Notably, flood volume per unit of impervious area fluctuated over time and did not show a clear or proportional relationship with either the increase in total flood volume or the expansion of urban extent. This remarks the dominant role of "PLAND impervious surface" but also suggests the importance of further exploring how the dynamics of urban landscape patterns influence pluvial flooding during urban expansion.

3.2. *Overall relationship between changes in urban morphology and pluvial flooding*

The PDPs from the GAMs trained on data samples representing all levels of pre-expansion urban coverage are illustrated in Fig. 3. Across all three study areas, a consistent and statistically significant negative relationship is observed between changes in green space aggregation (i.e., ΔAI green space) and the changes in pluvial flood volume under most rainfall scenarios across varying return periods. Similarly, the edge complexity of impervious surfaces (i.e., ΔLSI impervious surfaces) also presents a negative relationship with Δflood volume. In contrast, changes in green space shape complexity (i.e., ΔAWMSI green space) exhibit positive associations with Δflood volume. Although "ΔPLAND impervious ratio" shows statistical significance ($p < 0.001$) with Δflood volume across all the study areas with all the rainfall return period events, their wide 95 % confidence interval (CI) indicates great uncertainty in the estimated relationship or effect, when trained with all the data samples.

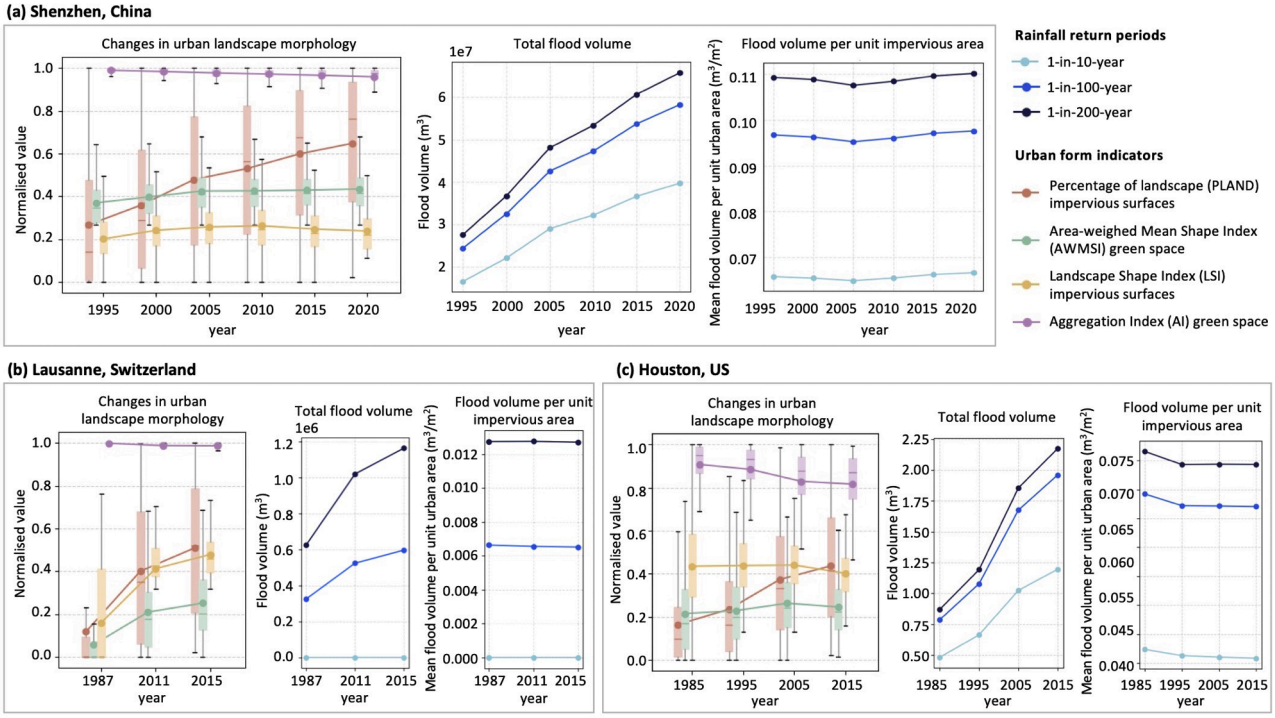

Fig. 2. Statistical summary of temporal changes in urban landscape morphology and pluvial flooding during urban expansion across the three study areas: (a) Shenzhen, China; (b) Lausanne, Switzerland; and (c) a suburban area in Houston, US. In each subfigure, the box plot on the left illustrates changes in the distribution of landscape morphological indicators over time; the line chart in the middle shows the total flood volume across the entire urban area for each year; and the right line chart presents the flood volume per unit impervious area.

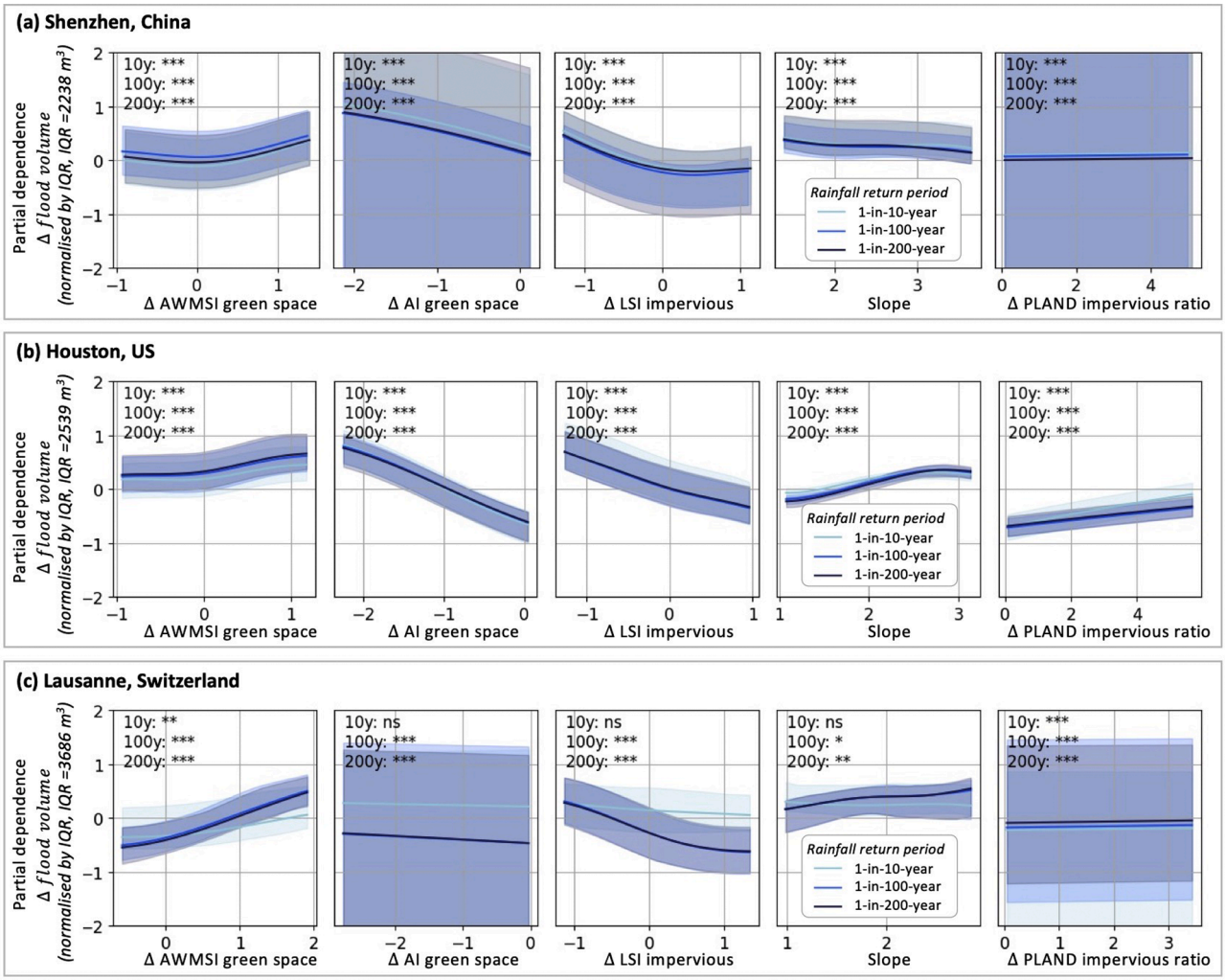

Fig. 3. Partial dependence plots showing the marginal effects of changes in urban landscape morphological indicators on pluvial flood volume, simulated using three return periods for rainfall extremes, across the three study areas: (a) Shenzhen, China; (b) a suburban area in Houston, US; and (c) Lausanne, Switzerland. The plots in each subfigure were generated using all data samples within each study area. *** indicates $p < 0.001$; ** indicates $p < 0.01$; * indicates $p < 0.05$; · indicates $p < 0.1$; ns denotes a non-significant result ($p \geq 0.1$).

3.3. Relationship between changes in urban morphology and pluvial flooding at different urbanisation stages

To gain an in-depth understanding of the intricate relationships between the dynamics of urban landscape and pluvial flooding, we conducted an analysis using four stratified subsets based on pre-expansion urban coverage (i.e., <25 %, 25–50 %, 50–75 %, >75 %), which serves as a proxy for indicating the stage of urbanisation. It can be observed that the association between changes in urban morphological indicators and Δflood volume varies in magnitude across different levels of pre-expansion urban coverage in all three study areas (Figs. 4, 5, and 6).

Considering the results of low pre-expansion urban coverage (<25 %) in Shenzhen (Fig. 4a), "ΔAI green space" and "ΔLSI impervious surfaces" consistently emerged as relatively important indicators influencing Δflood volume across the three study areas. For instance, an increase in the normalised "ΔAI green space" from -1.0 to -0.5 is projected to decrease Δflood volume (1-in-100 year) from -0.59 to -1.37 relative to the average predicted Δflood volume, corresponding to a reduction in Δflood volume from -1391 m^3 to -3250 m^3 (Δ1853 m^3). "ΔLSI impervious surfaces" presents a relatively weaker negative relationship with Δflood volume, an increase from -1.0 to -0.5 is projected to decrease Δflood volume (1-in-100 year) from 0.66 to 0.59, corresponding to a reduction from 1574 m^3 to 1405 m^3 (Δ169 m^3). At this stage, "ΔPLAND impervious ratio" has minimal influence on Δflood volume. As pre-expansion urban coverage increases to 25–50 % (Fig. 4b), "ΔAI green space" remains significant but shows reduced effect sizes, an increase from -1.0 to -0.5 is projected to decrease Δflood volume (1-in-100 year) from -0.04 to -0.25, corresponding to a reduction in increased flood volume from -93 m^3 to -590 m^3 (Δ497 m^3), indicating a decreased flood-regulating capacity. Meanwhile, the influence of "ΔPLAND impervious ratio" begins to increase. With 50–75 % pre-expansion coverage (Fig. 4c), "ΔAI green space" continues to show negative correlations with flood volume, though both the strength and statistical significance of these associations further decline, the same increase from -1.0 to -0.5 is projected to decrease Δflood volume (1-in-100 year) from 0.02 to -0.08, corresponding to a reduction in decreased Δflood volume from 52 m^3 to -197 m^3 (Δ249 m^3), and the Δflood volume for >75 % pre-expansion coverage is projected to decrease from -0.11 to -0.12, which is from -259 to -281 m^3 (Δ22 m^3). At very high levels of urbanisation (>75 %) (Fig. 4d), the influence of all three morphological indicators of urban landscape becomes negligible, with confidence intervals approaching zero. In contrast, the "ΔPLAND impervious ratio" emerges as the dominant factor associated with Δflood volume.

Similar association patterns can also be observed in the results for Houston (Fig. 5) and Lausanne (Fig. 6). The association between changes

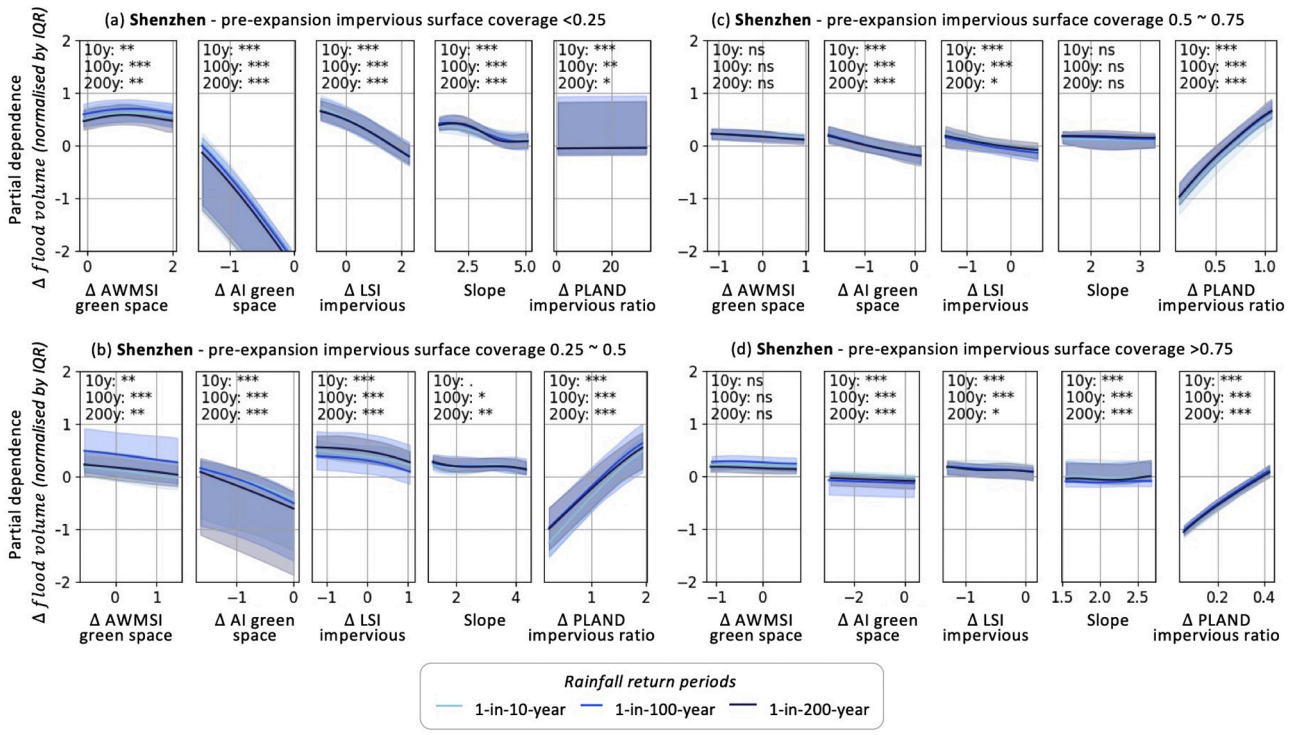

Fig. 4. Partial dependence plots showing the marginal effects of changes in urban landscape morphological indicators on pluvial flood volume, simulated using three return periods for rainfall extremes, and data from the study areas in Shenzhen, China. Each subfigure presents plots generated from a subset of data samples grouped by the percentage of pre-expansion impervious surface coverage: (a) less than 25%; (b) between 25% and 50%; (c) between 50% and 75%; and (d) greater than 75%. *** indicates $p < 0.001$; ** indicates $p < 0.01$; * indicates $p < 0.05$; · indicates $p < 0.1$; ns denotes a non-significant result ($p \geq 0.1$).

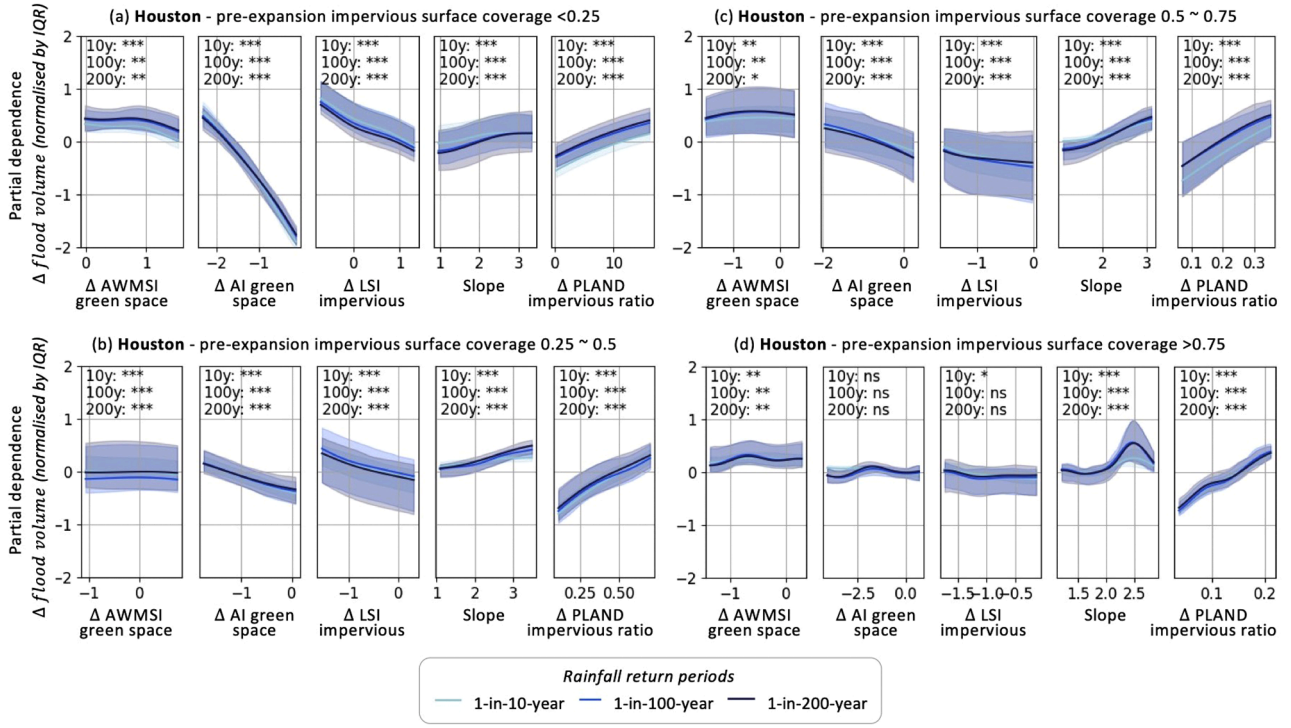

Fig. 5. Partial dependence plots showing the marginal effects of changes in urban landscape morphological indicators on pluvial flood volume, simulated using three return periods for rainfall extremes, and data from the study areas in Houston, US. Each subfigure presents plots generated from a subset of data samples grouped by the percentage of pre-expansion impervious surface coverage: (a) less than 25%; (b) between 25% and 50%; (c) between 50% and 75%; and (d) greater than 75%. *** indicates $p < 0.001$; ** indicates $p < 0.01$; * indicates $p < 0.05$; · indicates $p < 0.1$; ns denotes a non-significant result ($p \geq 0.1$).

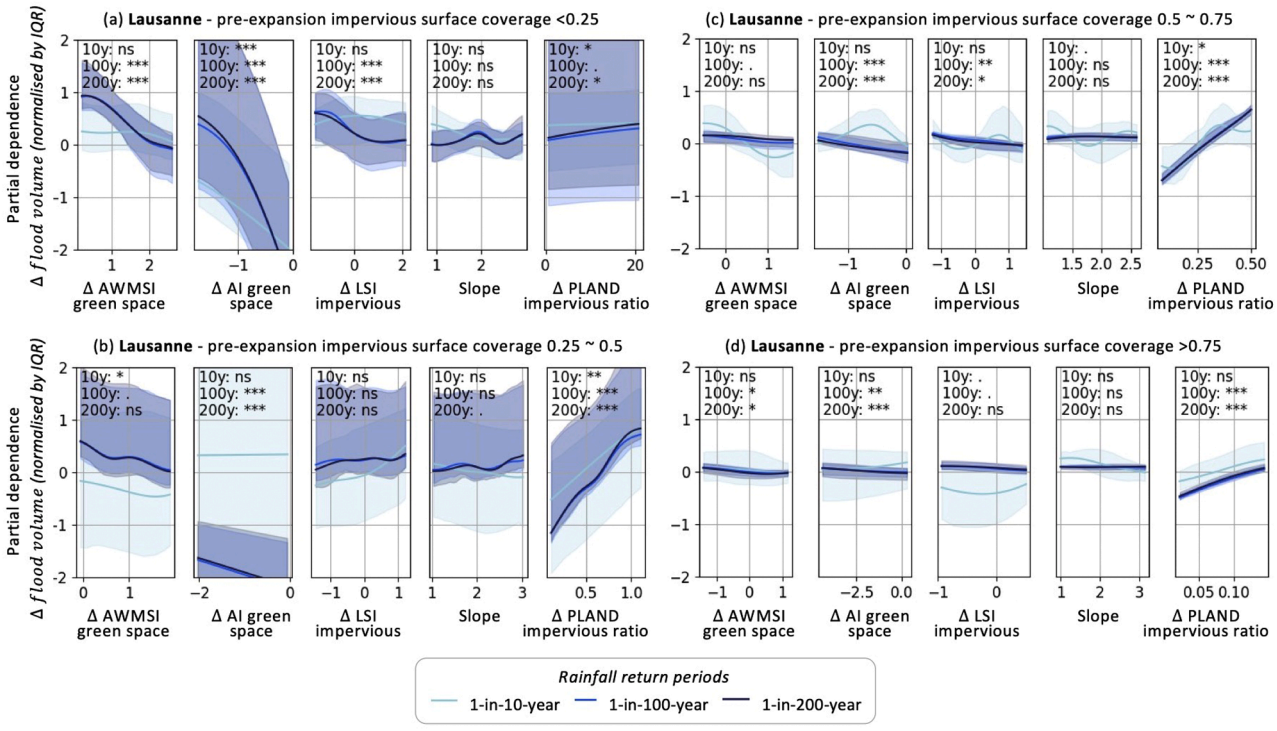

Fig. 6. Partial dependence plots showing the marginal effects of changes in urban landscape morphological indicators on pluvial flood volume, simulated using three return periods for rainfall extremes, and data from the study areas in Lausanne, Switzerland. Each subfigure presents plots generated from a subset of data samples grouped by the percentage of pre-expansion impervious surface coverage: (a) less than 25%; (b) between 25% and 50%; (c) between 50% and 75%; and (d) greater than 75%. *** indicates $p < 0.001$; ** indicates $p < 0.01$; * indicates $p < 0.05$; · indicates $p < 0.1$; ns denotes a non-significant result ($p \geq 0.1$).

in urban landscape morphology and Δflood volume is strongest at low levels of pre-expansion urban coverage and becomes negligible as urbanisation intensifies. In both Houston and Lausanne, the magnitudes of "ΔAI green space" and "ΔLSI impervious surfaces" also lose significance beyond 75 % pre-expansion urban coverage. Specifically, in Houston, an increase in the normalised "ΔAI green space" from -1.0 to -0.5 is projected to decrease the 1-in-100-year Δflood volume from -0.72 to -1.30 (Δ2299 m^3) for low pre-expansion urban coverage (<25 %), from -0.09 to -0.24 (Δ619 m^3) for coverage between 25 and 50 %, from 0.13 to -0.02 (Δ587 m^3) for coverage between 50 and 75 %, and only from 0.03 to -0.01 (Δ152 m^3) for areas with pre-expansion urban coverage exceeding 75 %. Additionally, while "ΔAWMSI green space" appears positively associated with Δflood volume in the full dataset, it does not exhibit a consistent directional association across the four stratified subsets under all rainfall scenarios and across all three cities.

A summary of the performance assessment of the GAM models is presented in Table 3, including models trained with the full dataset as well as those trained on stratified subsets. In all three cities, R^2 and adjusted R^2 values are consistently higher in the stratified models, indicating improved explanatory power when accounting for baseline urbanisation levels. This enhanced performance highlights the importance of stratifying by pre-expansion impervious coverage when modelling the hydrological impacts of urban morphological change, and further supports the presence of threshold effects whereby the influence of morphological indicators varies across different stages of urbanisation.

Additionally, we conducted two sensitivity tests to examine whether the results are sensitive to variations in (i) infiltration rates of impervious surfaces and (ii) rainfall intensity, using Houston and Shenzhen as representative cases. The tested infiltration rates span four drainage efficiency scenarios for Houston: 0 %, 30 %, 50 %, and 70 %, corresponding to infiltration rates of 0, 16, 26, and 36 mm/h, respectively (Figure C1, Appendix C). The results show that both the relative importance of morphological change indicators and the threshold effects remain consistent across these scenarios, indicating that the main conclusions are robust to the assumed drainage efficiency. For the second

Table 3
Performance of the GAM models across all study areas and rainfall scenarios, evaluated using all data samples as well as subsets grouped by pre-expansion urban coverage (i.e., less than 25%, 25–50%, 50–75%, and over 75%). Model performance is assessed on the test set using R^2 (first row) and adjusted R^2 (second row).

		Shenzhen, China					Houston, US					Lausanne, Switzerland				
		all	< 0.25	0.25-0.5	0.5-0.75	> 0.75	all	< 0.25	0.25-0.5	0.5-0.75	> 0.75	all	< 0.25	0.25-0.5	0.5-0.75	> 0.75
1-in-10 year	R^2	0.37	0.78	0.91	0.85	0.87	0.80	0.91	0.93	0.95	0.89	0.39	0.65	0.63	0.57	0.44
	adj. R^2	0.37	0.78	0.91	0.84	0.87	0.80	0.91	0.93	0.94	0.88	0.35	0.55	0.43	0.21	0.29
1-in-100 year	R^2	0.34	0.75	0.87	0.78	0.81	0.70	0.86	0.89	0.84	0.70	0.56	0.72	0.91	0.91	0.86
	adj. R^2	0.34	0.74	0.87	0.77	0.81	0.70	0.85	0.89	0.82	0.67	0.53	0.65	0.87	0.84	0.82
1-in-200 year	R^2	0.35	0.74	0.86	0.80	0.80	0.67	0.84	0.89	0.79	0.67	0.54	0.65	0.93	0.84	0.77
	adj. R^2	0.35	0.73	0.86	0.79	0.79	0.67	0.83	0.88	0.77	0.63	0.50	0.55	0.89	0.71	0.71

sensitivity test with perturbations on rainfall intensity, using Shenzhen as the study area and the 1-in-100-year, 30 min rainfall event as the baseline, we perturbed rainfall intensity by ±20 %. As shown in Figure C2 (Appendix C), the partial dependence patterns and the overall model performance remain consistent and stable across the -20 % (169 mm/h), baseline (200 mm/h), and +20 % (240 mm/h) rainfall scenarios, indicating that the conclusions are not sensitive to moderate variations in storm intensity.

3.4. Sensitivity test with synthetic urban expansion scenarios

Since the statistical analysis identified "ΔAI green space" and "ΔLSI impervious surfaces" as key indicators of changes in flood volume, as shown in the stratified analysis across the three study areas (Figs. 4–6), we further focused on them by examining their effects using synthetic urban expansion scenarios (Fig. 7). The initial urban patch had a pre-expansion urban coverage of 26 %, with the corresponding simulated flood volume as 63835 m^3 for a 30 min rainfall duration with a 1-in-100-year return period. Using this as a baseline, we generated eight urban expansion scenarios, each resulting in approximately a 20 % increase in impervious surface area (i.e., reaching 46 % total urban coverage), but differing in landscape morphology. These scenarios were specifically designed to vary the aggregation and edge complexity of landscape patterns, with the goal of reflecting the effects of changing "ΔAI green space" and "ΔLSI impervious surfaces" on flood volume. These scenarios systematically varied two key indicators by manually adjusting the urban expansion patterns, while keeping the total expansion area constant to enable disentangling the influence of landscape configuration from that of total impervious area, which is a dominant control. Connectivity was not explicitly enforced, as green-space connectivity represents a composite property of urban form that cannot be fully isolated or represented by a single quantitative indicator.

The eight scenarios correspond to typical urban growth modes, including compact corridor development (i.e., scenarios 1 and 2), compact outward expansion (i.e., scenarios 5 and 6), and irregular edge expansion (i.e., scenarios 3, 4, 7, and 8). These different types of scenarios not only reflect the variations in ΔAI and ΔLSI but also capture a realistic spectrum of potential urban expansion pathways. In this manner, the synthetic test enables a quantitative comparison of how multiple morphological metrics interact in shaping flood response. By generating expansion scenarios with varying "ΔAI green space" values that represent different urban growth typologies, we necessarily induced variations in "ΔLSI impervious surfaces" and other form indicators, which were also quantified. Changes in these indicators and associated Δflood volume can be compared to reveal how similar changes in one metric may lead to distinct hydrological responses under different co-varying morphological conditions.

As shown in the scatter plot in Fig. 7, "ΔAI green space" and "ΔLSI impervious surfaces" tend to be negatively correlated across the eight scenarios. This is likely because newly expanded urban areas often fragment existing green spaces, reducing their aggregation (ΔAI) while simultaneously increasing the edge complexity of impervious areas

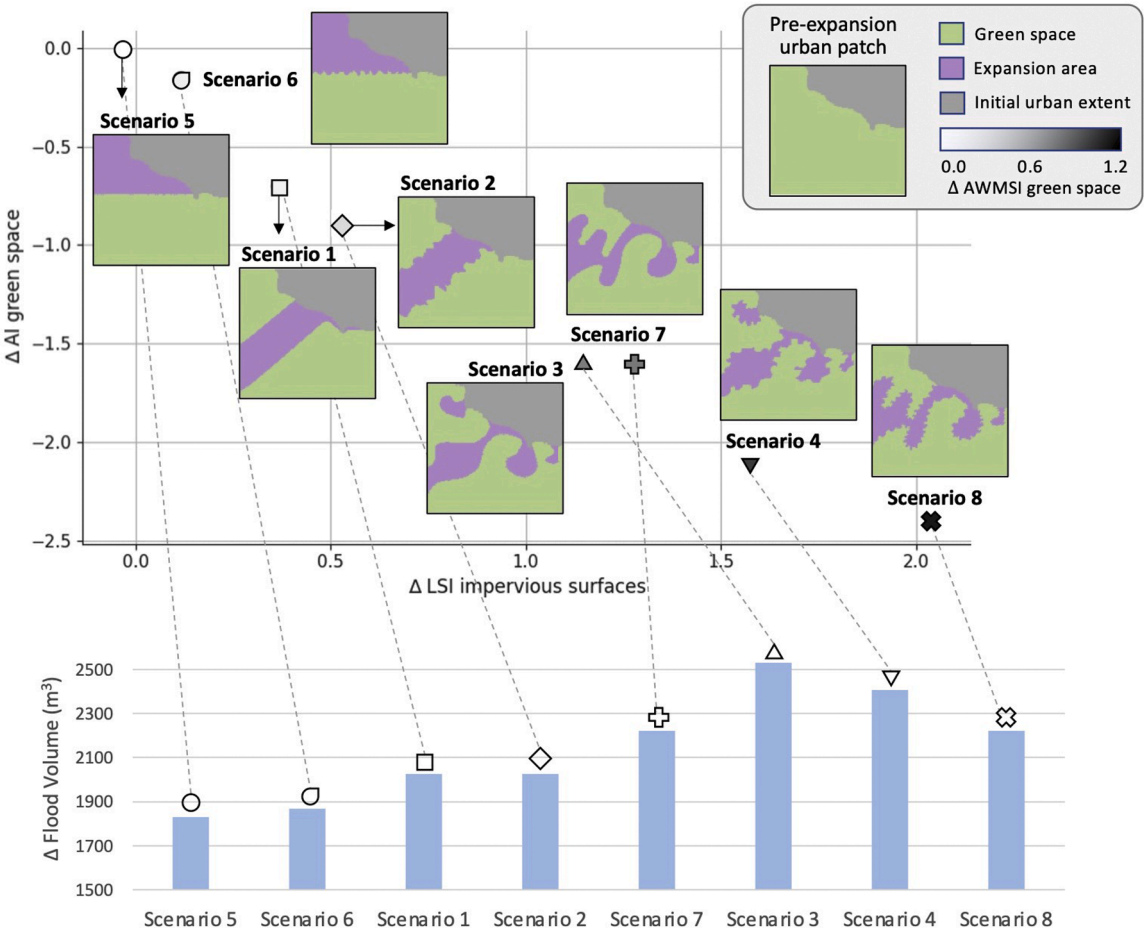

Fig. 7. Sensitivity analysis of how variations in key urban morphological indicators affect simulated flood volumes using eight synthetic urban expansion scenarios. The top scatter plot shows the eight scenarios, each represented by distinct markers, with values of three indicators, "ΔAI green space," "ΔLSI impervious surfaces," and "ΔAWMSI green space" (indicated by the grey colour gradient). The bottom bar plot presents the corresponding changes in flood volume (Δ Flood Volume) across the eight scenarios.

(ΔLSI). The lower bar chart in Fig. 7 presents the corresponding Δflood volume for each scenario. It is evident that scenarios that maintain green space compactness, tend to result in relatively lower increases in flood volumes. For instance, scenarios 5 and 6 feature small changes in "ΔAI green space" (around -0.2), the 20 % increase in impervious surface in these two scenarios results in Δflood volumes of approximately +1850 m^3. In contrast, scenario 3, with a much larger reduction in "ΔAI green space" (around -1.5), representing more fragmented and irregular green space, yields a Δflood volume of about +2500 m^3, which is around 35 % higher than scenario 5.

The negative association between "ΔLSI impervious surfaces" and Δflood volume can be observed when comparing scenarios 3 and 7, which have very similar values of "ΔAI green space", but scenario 3 has a lower value of "ΔLSI impervious surfaces" and exhibits higher Δflood volume than scenario 7. This suggests that when green spaces face a similar level of fragmentation, increased edge complexity of impervious surfaces may help mitigate flood volume increases.

Notably, the effects of "ΔAI green space" on Δflood volume are not strictly linear. For instance, although scenario 8 exhibits the largest reduction in "ΔAI green space" (around -2.4), the corresponding Δflood volume is around +2200 m^3, which is about 12 % lower than that of scenario 3, whereas scenario 3 features a smaller reduction in "ΔAI green space". This may be due to the higher "ΔLSI impervious surfaces" values in scenario 8 partially offset its negative impact of reduced green space aggregation. This observation may suggest that, while "ΔAI green space" and "ΔLSI impervious surfaces" are each negatively associated with Δflood volume, improvements in one metric may come at the expense of the other.

4. Discussion

4.1. Threshold effects of green space morphology

Among all the tested morphological indicators of urban landscape changes, "ΔAI green space" appears to be a strong and consistent influence on change in flood volume in stratified analysis across all three cities, underscoring the critical role of green space connectivity and aggregation in flood regulation, which aligns with existing studies (Dai & Tan, 2024; Kim & Park, 2016; Zhang et al., 2024). This relationship likely arises because aggregated and well-connected green spaces enhance infiltration and surface water retention disrupting the concentration of runoff, thereby reducing flood volume. In contrast, fragmented or isolated green patches do not disrupt hydrological continuity and lead to faster surface flow accumulation.

However, the effects of "ΔAI green space" on Δflood volume vary across different levels of pre-expansion urban coverage. The stratified analysis reveals that the influence of green space morphology on pluvial flooding is most pronounced in areas with low to moderate urban coverage (e.g., <50 %), whereas the effects become negligible when urbanisation intensifies (e.g., >75 %) across all three rainfall return periods. As reported in the result analysis, in Shenzhen, a 0.5-unit increase (from -1.0 to -0.5) in "ΔAI green space" is projected to reduce the 1-in-100-year Δflood volume by 1853, 497, 249, and 22 m^3 for pre-expansion urban coverage levels of <25 %, 25–50 %, 50–75 %, and >75 %, respectively. The corresponding projected reductions in Houston are 2299, 619, 587, and 152 m^3, respectively. Moreover, similar to "ΔAI green space", the negative correlation between "ΔLSI impervious surfaces" and Δflood volume also diminished as urbanisation intensifies (i.e., >75 %).

These results highlight the limitation in existing literature that relies on broad classifications of urban expansion (e.g., infill, leapfrog, edge expansion) to study flood dynamics. The misaligned findings reported by recent studies, some identifying leapfrog and edge expansion as more flood-prone, while others link infill development to greater flood exposure (Idowu & Zhou, 2023; Mabrouk et al., 2024), may arise from the fact that such broad typologies mask important heterogeneities in landscape morphological characteristics and baseline pre-expansion urban coverage.

These patterns also suggest a threshold effect, where the flood mitigation benefits of an optimal green space morphology substantially decline, this is the case when urban coverage exceeds a critical level (e.g., 50–75 %). Such variations and the threshold effect may be attributed to the different spatial flexibility available for maintaining and configuring green spaces under varying degrees of impervious coverage. In areas with low urban coverage, there is sufficient spatial flexibility to maintain aggregated green spaces (i.e., higher "ΔAI green space"), which are associated with reduced increases in flood volume. This highlights the importance of preserving compact and well-connected green spaces from the early stages of urban expansion, where their benefits of pluvial flooding mitigation are most effective. In contrast, in highly urbanised areas, green spaces are already scarce and fragmented. Subsequent urbanisation often takes the form of infill development (Sun et al., 2013), which further disrupts green space connectivity and limits its function as a green space network. As a result, pluvial flooding in such areas tends to be primarily governed by topography and the extent of impervious surfaces. The stratified analysis provides complementary insights by showing that when pre-expansion urban coverage is similar and the aggregation level is controlled, greater edge complexity of impervious surface may also limit flood volume increases.

Notably, the thresholds identified here should not be interpreted as a universal break points. Rather, they represent emergent patterns observed through stratified analysis, in which indicator performance changes across different levels of urban impervious coverage. The magnitude of these performances and the exact threshold are likely to vary with flood intensity and cities, and may also be affected by city-specific climate, geomorphological and socio-cultural contexts. For instance, local climate determines rainfall intensity, while socio-cultural factors can shape variations in urban form characteristics, which in turn may affect flow paths and infiltration efficiency. These context-specific factors jointly modulate when critical thresholds can be reached, making exact thresholds dependent on the properties of each city, which highlights the importance of context-specific planning to support long-term flood resilience.

These results also bring practical implications for urban planning. During the process of urban expansion, a cap on impervious surface coverage should be considered to maximise the effectiveness of green infrastructure in mitigating flood risks. The effective implementation of an impervious surface cap can be facilitated through cross-departmental collaboration and appropriate incentive programmes. The results of this study highlight how important is the coordination among the various municipal agencies responsible for urban planning in order to achieve an effective impact of green space management. Institutionalised planning frameworks and tax incentives or subsidies to developers could, for instance, foster the aggregation of green spaces. Moreover, in highly urbanised areas, planning should prioritise reducing or replacing impervious surfaces with pervious ones and strategically forming or connecting green spaces to help restore flow disruption and enhance infiltration capacity, such as retrofitting paved surfaces (e.g., parking lots, low-traffic roads) with permeable materials, decreasing total impervious surface to maximise the benefits of positive urban form (e.g., aggregated green space).

4.2. Interplay between green space morphology indicators

While both "ΔAI green space" and "ΔLSI impervious surfaces" are associated with Δflood volume, the sensitivity tests with synthetic scenarios demonstrate that the influence of these morphological indicators on flood volume is not strictly linear. For instance, less fragmented green space may not always result in reduced flood volume (e.g., scenarios 3 and 8). This can be attributed to the fact that changes in landscape morphology rarely affect a single indicator in isolation. Instead, improving one morphological indicator often comes at the expense of

another. For instance, increasing the edges of impervious surface, aiming for a smaller Δflood volume, may result in increased green space fragmentation (i.e., lower "ΔAI green space"), which can partially offset the impact of increased edge complexity, and may lead to a larger Δflood volume.

Such an interplay also suggests that implementing green infrastructure for flood mitigation is not a straightforward task that can be achieved by simply maximising individual morphological characteristics. This highlights the risk of deriving planning recommendations directly from correlation analyses and assuming a linear relationship between individual green space metrics and flood risk. Such assumptions can be misleading and could suggest that altering a specific green space characteristic will result in a proportional reduction in flooding. Instead, these relationships in real-world scenarios are more nuanced, context-dependent, and nonlinear.

Thus, urban planning for flood mitigation should move beyond simple metrics or one-size-fits-all generalisations and test any specific intervention in the local context of urban fabric, possibly using high-resolution hydrological and hydraulic models. However, even in absence of a detailed and local analysis, a more integrated approach, such as preserving the aggregation of green space while allowing for manageable increases in edge complexity, is likely to create some flood reduction benefit. Recognising and navigating these trade-offs would be essential for designing green areas that remain effective across different stages of urbanisation.

4.3. Limitations and future work

While this study provides a robust comparative analysis across three diverse urban contexts using three different return periods for rainfall extremes, several simplifications and limitations should be acknowledged. First, not all the factors that influence surface runoff and flood behaviour in real-world scenarios were included in the flood simulations, certain factors were intentionally simplified to investigate the flood response of large-scale urban morphological changes under a controlled and comparable framework. In particular, the simulations were primarily based on the spatial patterns of surface imperviousness and homogenous rainfall over the domain. It means we did not account for various urban features, including city roughness, which may influence rainfall patterns (Torelló-Sentelles et al., 2025; Yang et al., 2024). Surface imperviousness was simplified into two classes, impervious and pervious surfaces, this may overlook fine-scale differences in infiltration capacity across different soils and land covers, such as gravel areas or vegetated pavements, but allows a variable-controlled comparison across three distinct urban areas. Also, the heterogeneity of the underground drainage infrastructure was not explicitly considered. Instead, drainage capacity was approximated through a reference infiltration rate of impervious areas, which is assumed to represent the drainage capacity of a standardly designed sewage system. While this approach enables a controlled and comparable setup across cities, it simplifies local effects and surface-subsurface interactions in flood simulations. Moreover, rainfall intensity was assumed spatially homogeneously in all flood simulations, this may underestimate the influence of spatially heterogeneous rainfall patterns on flood dynamics (Peleg et al., 2017). Besides, all rainfall scenarios in this study were set up with a 30-minute rainfall duration, which provides consistency for cross-city comparison and a realistic setup for short, high-intensity pluvial flood events, but it does not correspond to the time of concentration of any specific sub-catchment in the domain. Additionally, under prolonged rainfall conditions, the water storage capability of green spaces may decline as soils gradually reach saturation, potentially reducing their flood mitigation effect.

This study adopts flood volume as the metric to examine the effect of urban morphological changes on pluvial flooding. While flood volume captures the overall performance of flood depth and inundation area, it lacks direct fine-grained information on floodwater depth at specific locations. In addition, although synthetic scenarios can control the effects of certain influencing variables (e.g., the proportion of pre-expansion, the amount of increased urban coverage), they are unlikely to exhaustively capture all possible morphological configurations of urban landscape in real-world urban transformations, for instance, fine-grained interactions between different land use or vegetation types observed in actual cities are largely underrepresented in synthetic analyses.

It should also be noted that, since this study focuses on relative flood responses to urban form changes under controlled design rainfall scenarios rather than on reproducing specific historical flood events. Observations of water depth and flood extent of real events over cities are rarely available and are often quite discontinuous in space and time making any validation very challenging (Ivanov et al., 2021). Furthermore, real-world pluvial events across cities will occur with different rainfall intensities and return periods of the event, and different drainage conditions, even when data are available, calibrating for those events could introduce event-specific biases and undermine the goal of establishing a consistent comparative framework, which is the ultimate goal of this study. Nevertheless, a sensitivity analysis was conducted by varying rainfall intensity and infiltration rates representing drainage efficiency to mimic real-world conditions. The results indicate that reasonable variations in these key factors do not affect the overall consistency of the results (Appendix C).

Additionally, certain city-specific factors, such as average elevation and total urban area, may affect the absolute magnitude of correlation between changes in urban form indicators and flood response. Although our analysis focused on temporal changes within each city, where the DEM was constant and pre-expansion impervious coverage was addressed through stratified analysis, these contextual differences may still influence the magnitude of the correlations observed. Therefore, our results provide indications of relative feature importance and directional effects rather than direct absolute comparisons between cities. In addition, flood-mitigation infrastructures associated with socio-economic conditions, investments and management capacity vary across cities and were not included in the analysis. This limitation may overlook how variations in governance, maintenance, and planning policies affect the effectiveness of green infrastructure and the overall city flood response.

While this study covers three urban areas with diverse terrain features and climatic conditions, which enhances the generalizability of the findings, we acknowledge that the conclusions may not be fully applicable to cities with markedly different urban forms or climate conditions. Future studies could therefore further test generalisability by examining a broader range of cities experiencing varied intensities of urbanisation as well as greater geographic and climatic diversity. A further area of future research would also concern the investigation about whether the observed relationships remain consistent under projected rainfall scenarios that account for altered spatial and temporal rainfall patterns, as well as potential climate change effects and changes in the long-term water storage capacity of green spaces under prolonged rainfall durations or after prolonged dry periods. Such explorations may help inform strategies to ensure the continued effectiveness of green infrastructure as climate conditions evolve and extreme weather patterns change. Future research could also incorporate vertical urban form (e.g., buildings) to examine its potential indirect effects on pluvial flooding when time-series data on vertical urban form changes become available. Finally, future research could further corroborate the robustness of this framework and the results of this study by testing the simulations for specific city context where multiple flood data are available, including citizen-science reports, gauge-based water-level observations, and remotely sensed inundation maps for a range of events encompassing scenarios consistent with those analysed in this study. With the increasing importance of urban greening, the continuing development of high-frequency remote sensing technologies and the growing use of citizen-science approaches, such validation may become increasingly feasible in the future.

5. Conclusion

This study examined how changes in urban landscape morphology influence pluvial flooding in the process of urban expansion, using multi-temporal data from Shenzhen (1995-2020), Lausanne (1987-2015), and suburban Houston (1985-2015). By employing GAMs to link temporal changes in urban landscape morphology with flood volume variations simulated under 1-in-10-, 1-in-100-, and 1-in-200-year rainfall events, the study identified key morphological indicators that influence the magnitude of increased flood volume during urban expansion.

Among the analysed indicators of urban form changes, the changes in aggregation of green space (ΔAI) and edge complexity of impervious surfaces (ΔLSI) emerged as important indicators associated with the changes in flood volume. Across the three cities, "ΔAI green space" and "ΔLSI impervious surfaces" exhibited a statistically significant negative relationship with flood volume ($p < 0.01$ in most cases). This effect was further quantified in sensitivity experiments with synthetic scenarios, in which compact and aggregated green space configurations produced flood volume increases of ~1850 m^3 under a 20 % expansion of impervious area, whereas fragmented configurations led to increases of ~2500 m^3 despite the same total impervious gain.

Another key finding is the presence of a threshold effect based on pre-expansion urban coverage. The influence of green space morphology on pluvial flooding is more pronounced in areas with low to moderate pre-expansion urban coverage (e.g., <50 %), and diminishes beyond a certain urbanisation threshold (e.g., >75 %), where imperviousness becomes a more dominant factor influencing pluvial flooding. In support of this, the stratified GAM models achieved consistently higher explanatory power (R^2 often >0.75 compared to <0.40 in the full-sample models), underscoring the importance of stratifying by baseline urbanisation levels and confirming that the influence of morphological indicators varies across different stages of urbanisation.

The overall consistent patterns across the three study areas demonstrates some degree of generalisability of this threshold effect, but the specific threshold values may vary in distinctive urban context. These results underscore the importance of preserving compact, aggregated green spaces from the early stages of urban growth to mitigate pluvial floods and thus can guide planning of future urban expansions.

CRediT authorship contribution statement

Yue Zhu: Writing – original draft, Visualization, Validation, Software, Methodology, Investigation, Formal analysis, Data curation, Conceptualization. **Paolo Burlando:** Writing – review & editing, Supervision, Resources, Methodology, Funding acquisition, Conceptualization. **Ye Zhang:** Writing – review & editing. **Dengkai Chi:** Writing – review & editing. **Jing Wang:** Writing – review & editing. **Yeshan Qiu:** Writing – review & editing. **Matteo Bonatesta:** Data curation. **Wenyue Zou:** Writing – review & editing, Data curation. **Christian Geiß:** Writing – review & editing, Resources. **Puay Yok Tan:** Writing – review & editing, Supervision, Funding acquisition. **Simone Fatichi:** Writing – review & editing, Supervision, Methodology, Funding acquisition, Conceptualization.

Declaration of competing interest

The authors declare that they have no known competing financial interests or personal relationships that could have appeared to influence the work reported in this paper.

Acknowledgements

This research was funded in part by the Future Cities Lab Global programme. Future Cities Lab Global is supported and funded by the National Research Foundation, Prime Minister's Office, Singapore under its Campus for Research Excellence and Technological Enterprise (CREATE) programme and ETH Zurich (ETHZ), with additional contributions from the National University of Singapore (NUS), Nanyang Technological University (NTU), and the Singapore University of Technology and Design (SUTD). We gratefully acknowledge the Centre for Water Systems at the University of Exeter for providing an academic license, enabling access to the CAFlood Pro software.

Supplementary materials

Supplementary material associated with this article can be found, in the online version, at doi:10.1016/j.scs.2025.107018.

Data availability

Data will be made available on request.

References

Alberti, M., & Marzluff, J. M. (2004). Ecological resilience in urban ecosystems: Linking urban patterns to human and ecological functions. *Urban Ecosystems, 7*(3), 241–265. https://doi.org/10.1023/B:UECO.0000044038.90173.c6

Angel, S., Parent, J., Civco, D. L., & Blei, A. M. (2012). *Atlas of Urban Expansion*. Cambridge MA: Lincoln Institute of Lang Policy.

Baida, M. E., Chourak, M., & Boushaba, F. (2024). Flood mitigation and water resource preservation: Hydrodynamic and SWMM simulations of nature-based solutions under climate change. *Water Resources Management*. https://doi.org/10.1007/s11269-024-04015-3

Balaian, S. K., Sanders, B. F., & Abdolhosseini Qomi, M. J. (2024). How urban form impacts flooding. *Nature Communications, 15*(1), 6911. https://doi.org/10.1038/s41467-024-50347-4

Broitman, D., & Koomen, E. (2015). Residential density change: Densification and urban expansion. *GeographyRN: Urban Processes (Sub-Topic)*. https://doi.org/10.1016/j.compenvurbsys.2015.05.006

Butler, D., Digman, C. J., Makropoulos, C., & Davies, J. W. (2018). *Urban Drainage* (4th edition). Boca Raton: CRC Press.

Chakraborty, S., Dadashpoor, H., Novotný, J., Maity, I., Follmann, A., Patel, P., … Pramanik, S. (2022). In pursuit of sustainability – Spatio-temporal pathways of urban growth patterns in the world's largest megacities. *Cities*. https://doi.org/10.1016/j.cities.2022.103919

Dai, W., & Tan, Y. (2024). Study on multi-scenario rain-flood disturbance simulation and resilient blue-green space optimization in the pearl river delta. *Buildings*. https://doi.org/10.3390/buildings14123797

DHI. (2013). *MIKE FLOOD –1D-2D Modelling – User Manual*.

Dibble, J., Prelorendjos, A., Romice, O., Zanella, M., Strano, E., Pagel, M., & Porta, S. (2019). On the origin of spaces: Morphometric foundations of urban form evolution. *Environment and Planning B: Urban Analytics and City Science, 46*, 707–730. https://doi.org/10.1177/2399808317725075

Fenta, A., Yasuda, H., Haregeweyn, N., Belay, A. S., Hadush, Z., Gebremedhin, M. A., & Mekonnen, G. (2017). The dynamics of urban expansion and land use/land cover changes using remote sensing and spatial metrics: The case of Mekelle City of northern Ethiopia. *International Journal of Remote Sensing, 38*, 4107–4129. https://doi.org/10.1080/01431161.2017.1317936

Fowler, H. J., Lenderink, G., Prein, A. F., Westra, S., Allan, R. P., Ban, N., … Zhang, X. (2021). Anthropogenic intensification of short-duration rainfall extremes. *Nature Reviews Earth & Environment, 2*(2), 107–122. https://doi.org/10.1038/s43017-020-00128-6

GEO. (2023). GEO technical guidance notes No. 30 (TGN 30) updated intensity-duration-frequency curves with provision for climate change for slope drainage design. Retrieved 3 June 2025, from https://www.cedd.gov.hk/eng/publications/geo/geo-technical-guidance-notes/index.html.

Gironás, J., Roesner, L. A., Rossman, L. A., & Davis, J. (2010). A new applications manual for the Storm Water Management Model (SWMM). *Environmental Modelling & Software, 25*(6), 813–814. https://doi.org/10.1016/j.envsoft.2009.11.009

Goldstein, A., Kapelner, A., Bleich, J., & Pitkin, E. (2013). Peeking inside the black box: Visualizing statistical learning with plots of individual conditional expectation. *Journal of Computational and Graphical Statistics, 24*, 44–65. https://doi.org/10.1080/10618600.2014.907095

Gomez-Rubio, V. (2018). Generalized additive models: An introduction with R (2nd Edition). *Journal of Statistical Software, 86*, 1–5. https://doi.org/10.18637/jss.v086.b01

Guidolin, M., Chen, A. S., Ghimire, B., Keedwell, E. C., Djordjević, S., & Savić, D. A. (2016). A weighted cellular automata 2D inundation model for rapid flood analysis. *Environmental Modelling & Software, 84*, 378–394. https://doi.org/10.1016/j.envsoft.2016.07.008

Huang, Y., Tian, Z., Ke, Q., Liu, J., Irannezhad, M., Fan, D., … Sun, L. (2020a). Nature-based solutions for urban pluvial flood risk management. *Wiley Interdisciplinary Reviews: Water, 7*. https://doi.org/10.1002/wat2.1421

Huang, Y., Tian, Z., Ke, Q., Liu, J., Irannezhad, M., Fan, D., … Sun, L. (2020b). Nature-based solutions for urban pluvial flood risk management. *WIREs Water, 7*(3), e1421. https://doi.org/10.1002/wat2.1421

Idowu, D., & Zhou, W. (2023). Global megacities and frequent floods: Correlation between urban expansion patterns and urban flood hazards. *Sustainability, 15*(3), 2514. https://doi.org/10.3390/su15032514

Ivanov, V. Y., Xu, D., Dwelle, M. C., Sargsyan, K., Wright, D. B., Katopodes, N., … Bras, R. L. (2021). Breaking down the computational barriers to real-time urban flood forecasting. *Geophysical Research Letters, 48*(20). https://doi.org/10.1029/2021GL093585. e2021GL093585.

Jian, W., Li, S., Lai, C., Wang, Z., Cheng, X., Lo, E., & Pan, T. (2020). Evaluating pluvial flood hazard for highly urbanised cities: A case study of the Pearl River Delta Region in China. *Natural Hazards, 105*, 1691–1719. https://doi.org/10.1007/s11069-020-04372-3

Kim, H., & Park, Y. (2016). Urban green infrastructure and local flooding: The impact of landscape patterns on peak runoff in four Texas MSAs. *Applied Geography, 77*, 72–81. https://doi.org/10.1016/J.APGEOG.2016.10.008

Kim, J., Warnock, A., Ivanov, V. Y., & Katopodes, N. D. (2012). Coupled modeling of hydrologic and hydrodynamic processes including overland and channel flow. *Advances in Water Resources, 37*, 104–126. https://doi.org/10.1016/j.advwatres.2011.11.009

Li, F., Zheng, W., Wang, Y., Liang, J., Xie, S., Guo, S., … Yu, C. (2019). Urban green space fragmentation and urbanization: A spatiotemporal perspective. *Forests*. https://doi.org/10.3390/F10040333

Li, H., Liu, Y., Zhang, H., Xue, B., & Li, W. (2021). Urban morphology in China: Dataset development and spatial pattern characterization. *Sustainable Cities and Society, 71*. https://doi.org/10.1016/J.SCS.2021.102981

Li, L., Uyttenhove, P., & Eetvelde, V. (2020). Planning green infrastructure to mitigate urban surface water flooding risk – A methodology to identify priority areas applied in the city of Ghent. *Landscape and Urban Planning, 194*. https://doi.org/10.1016/j.landurbplan.2019.103703

Li, Y., Ji, C., Wang, P., & Huang, L. (2023). Proactive intervention of green infrastructure on flood regulation and mitigation service based on landscape pattern. *Journal of Cleaner Production*. https://doi.org/10.1016/j.jclepro.2023.138152

Lin, J., Zhang, W., Wen, Y., & Qiu, S. (2023). Evaluating the association between morphological characteristics of urban land and pluvial floods using machine learning methods. *Sustainable Cities and Society, 99*, Article 104891. https://doi.org/10.1016/j.scs.2023.104891

Mabrouk, M., Han, H., Abdrabo, K. I., Mahran, M., AbouKorin, S. A. A., Nasralah, S., … Hafez, H. M. (2024). Spatial congruency or discrepancy? Exploring the spatiotemporal dynamics of built-up expansion patterns and flood risk. *The Science of the Total Environment*. https://doi.org/10.1016/j.scitotenv.2024.170019

Marconcini, M., Metz-Marconcini, A., Üreyen, S., Palacios-Lopez, D., Hanke, W., Bachofer, F., … Strano, E. (2020). Outlining where humans live, the World Settlement Footprint 2015. *Scientific Data, 7*(1), 242. https://doi.org/10.1038/s41597-020-00580-5

MeteoSwiss. (2022). Extreme value analyses. Retrieved 3 June 2025, from https://www.meteoswiss.admin.ch/climate/the-climate-of-switzerland/records-and-extremes/extreme-value-analyses.html.

Mitchell, M. G. E., & Devisscher, T. (2022). Strong relationships between urbanization, landscape structure, and ecosystem service multifunctionality in urban forest fragments. *Landscape and Urban Planning, 228*, Article 104548. https://doi.org/10.1016/j.landurbplan.2022.104548

Moustakis, Y., Papalexiou, S. M., Onof, C. J., & Paschalis, A. (2021). Seasonality, intensity, and duration of rainfall extremes change in a warmer climate. *Earth's Future, 9*(3). https://doi.org/10.1029/2020EF001824. e2020EF001824.

Muis, S., Güneralp, B., Jongman, B., Aerts, J. C. J. H., & Ward, P. J. (2015). Flood risk and adaptation strategies under climate change and urban expansion: A probabilistic analysis using global data. *Science of The Total Environment, 538*, 445–457. https://doi.org/10.1016/j.scitotenv.2015.08.068

National Weather Service. (2025). NOAA Atlas 14 point precipitation frequency estimates. Retrieved 3 June 2025, from https://hdsc.nws.noaa.gov/pfds/pfds_map_cont.html?bkmrk=tx.

Pallathadka, A., Sauer, J., Chang, H., & Grimm, N. B. (2022). Urban flood risk and green infrastructure: Who is exposed to risk and who benefits from investment? A case study of three U.S. Cities. *Landscape and Urban Planning, 223*, Article 104417. https://doi.org/10.1016/j.landurbplan.2022.104417

Peleg, N., Blumensaat, F., Molnar, P., Fatichi, S., & Burlando, P. (2017). Partitioning the impacts of spatial and climatological rainfall variability in urban drainage modeling. *Hydrology and Earth System Sciences, 21*(3), 1559–1572. https://doi.org/10.5194/hess-21-1559-2017

Qiang, Y., Zhang, L., & Xiao, T. (2020). Spatial-temporal rain field generation for the Guangdong-Hong Kong-Macau Greater Bay Area considering climate change. *Journal of Hydrology, 583*, Article 124584. https://doi.org/10.1016/j.jhydrol.2020.124584

Ran, Z., Gao, S., Zhang, B., Guo, C., Ouyang, X., & Gao, J. (2023). Non-linear effects of multi-dimensional urbanization on ecosystem services in mega-urban agglomerations and its threshold identification. *Ecological Indicators, 154*, Article 110846. https://doi.org/10.1016/j.ecolind.2023.110846

Rasool, U., Yin, X., Xu, Z., Rasool, M. A., Hussain, M., Siddique, J., & Hai, N. T. (2025). Quantifying pluvial flood simulation in ungauged urban area; A case study of 2022 unprecedented pluvial flood in Karachi, Pakistan. *Journal of Hydrology, 655*, Article 132905. https://doi.org/10.1016/j.jhydrol.2025.132905

Ravindra, K., Rattan, P., Mor, S., & Aggarwal, A. (2019). Generalized additive models: Building evidence of air pollution, climate change and human health. *Environment International, 132*. https://doi.org/10.1016/j.envint.2019.104987

Rentschler, J., Avner, P., Marconcini, M., Su, R., Strano, E., Vousdoukas, M., & Hallegatte, S. (2023). Global evidence of rapid urban growth in flood zones since 1985. *Nature, 622*, 87–92. https://doi.org/10.1038/s41586-023-06468-9

Rosenberger, L. J., Leandro, J., Pauleit, S., & Erlwein, S. (2021). Sustainable stormwater management under the impact of climate change and urban densification. *Journal of Hydrology*, 596. https://doi.org/10.1016/J.JHYDROL.2021.126137

Rossman, L.A. (2015). *Storm Water Management Model User's Manual Version 5.1*.

Su, J., Wang, M., Zhang, D., Yuan, H., Zhou, S., Wang, Y., & Razi, M. A. M. (2024). Integrating technical and societal strategies in Nature-based Solutions for urban flood mitigation in Guangzhou, a heritage city. *Ecological Indicators*. https://doi.org/10.1016/j.ecolind.2024.112030

Sun, C., Wu, Z., Lv, Z., Yao, N., & Wei, J. (2013). Quantifying different types of urban growth and the change dynamic in Guangzhou using multi-temporal remote sensing data. *Int. J. Appl. Earth Obs. Geoinformation, 21*, 409–417. https://doi.org/10.1016/j.jag.2011.12.012

Tan, X., Mai, Q., Chen, G., Liu, B., Wang, Z., Lai, C., & Chen, X. (2023). Intensity-duration-frequency curves in the Guangdong-Hong Kong-Macao Greater Bay Area inferred from the Bayesian hierarchical model. *Journal of Hydrology: Regional Studies, 46*, Article 101327. https://doi.org/10.1016/j.ejrh.2023.101327

Tian, Z., Lyu, X.-Y., Zou, H., Yang, H.-L., Sun, L., Pinya, M. S., … Smith, B. (2022). Advancing index-based climate risk assessment to facilitate adaptation planning: Application in Shanghai and Shenzhen, China. *Advances in Climate Change Research, 13*(3), 432–442. https://doi.org/10.1016/j.accre.2022.02.003

Torelló-Sentelles, H., Villarini, G., Koukoula, M., & Peleg, N. (2025). Impacts of urban dynamics and thermodynamics on convective rainfall across different urban forms. *Urban Climate, 62*, Article 102499. https://doi.org/10.1016/j.uclim.2025.102499

Tradowsky, J. S., Philip, S., Kreienkamp, F., Kew, S., Lorenz, P., Arrighi, J., … Wanders, N. (2023). Attribution of the heavy rainfall events leading to severe flooding in Western Europe during July 2021. *Climatic Change, 176*, 1–38. https://doi.org/10.1007/s10584-023-03502-7

Tran, V. N., Ivanov, V. Y., Huang, W., Murphy, K., Daneshvar, F., Bednar, J. H., … Wright, D. B. (2024). Connectivity in urbanscapes can cause unintended flood impacts from stormwater systems. *Nature Cities, 1*(10), 654–664. https://doi.org/10.1038/s44284-024-00116-7

United States Geological Survey. (2021). *United States Geological Survey 3D Elevation Program 1/3 arc-second Digital Elevation Model* [Data set]. doi:10.5069/G98K778D.

Vavassori, A., Giuliani, G., & Brovelli, M. A. (2023). Mapping Local Climate Zones in Lausanne (Switzerland) with Sentinel-2 and PRISMA imagery: Comparison of classification performance using different band combinations and building height data. *International Journal of Digital Earth* (world). Retrieved from https://www.tandfonline.com/doi/abs/10.1080/17538947.2023.2283485.

Wang, J., Huang, W., & Biljecki, F. (2024). Learning visual features from figure-ground maps for urban morphology discovery. *Computers, Environment and Urban Systems, 109*. https://doi.org/10.1016/j.compenvurbsys.2024.102076

Wang, Q., Liu, S., Liu, Y., Wang, F., Liu, H., & Yu, L. (2022). Effects of urban agglomeration and expansion on landscape connectivity in the river valley region, Qinghai-Tibet Plateau. *Global Ecology and Conservation*. https://doi.org/10.1016/j.gecco.2022.e02004

Wang, Y., Chen, A. S., Fu, G., Djordjević, S., Zhang, C., & Savić, D. A. (2018). An integrated framework for high-resolution urban flood modelling considering multiple information sources and urban features. *Environmental Modelling & Software, 107*, 85–95. https://doi.org/10.1016/j.envsoft.2018.06.010

Wiederkehr, M., & Möri, A. (2013). SwissALTI3D - A new tool for geological mapping. *Bulletin Fuer Angewandte Geologie, 18*, 61–69. https://doi.org/10.5169/seals-391140

Xu, C., Rahman, M., Haase, D., Wu, Y., Su, M., & Pauleit, S. (2020). Surface runoff in urban areas: The role of residential cover and urban growth form. *Journal of Cleaner Production, 262*, Article 121421. https://doi.org/10.1016/j.jclepro.2020.121421

Xu, L., You, H., Li, D., & Yu, K. (2016). Urban green spaces, their spatial pattern, and ecosystem service value: The case of Beijing. *Habitat International, 56*, 84–95. https://doi.org/10.1016/J.HABITATINT.2016.04.005

Yang, L., Yang, Y., Shen, Y., Yang, J., Zheng, G., Smith, J., & Niyogi, D. (2024). Urban development pattern's influence on extreme rainfall occurrences. *Nature Communications, 15*(1), 3997. https://doi.org/10.1038/s41467-024-48533-5

Zhang, B., Xie, G., Li, N., & Wang, S. (2015). Effect of urban green space changes on the role of rainwater runoff reduction in Beijing, China. *Landscape and Urban Planning, 140*, 8–16. https://doi.org/10.1016/j.landurbplan.2015.03.014

Zhang, W., Qiu, S., Lin, Z., Chen, Z., Yang, Y., Lin, J., & Li, S. (2024). Assessing the influence of green space morphological spatial pattern on urban waterlogging: A case study of a highly-urbanized city. *Environmental Research*. https://doi.org/10.1016/j.envres.2024.120561

Zhu, L., Emanuel, K., & Quiring, S. M. (2021a). Elevated risk of tropical cyclone precipitation and pluvial flood in Houston under global warming. *Environmental Research Letters, 16*(9), Article 094030. https://doi.org/10.1088/1748-9326/ac1e3d

Zhu, Y., Burlando, P., Tan, P. Y., Blagojevic, J., & Fatichi, S. (2024). Investigating the influence of urban morphology on pluvial flooding: Insights from urban catchments in England (UK). *Science of The Total Environment, 953*, Article 176139. https://doi.org/10.1016/j.scitotenv.2024.176139

Zhu, Y., Geiß, C., & So, E. (2021b). Image super-resolution with dense-sampling residual channel-spatial attention networks for multi-temporal remote sensing image

classification. *International Journal of Applied Earth Observation and Geoinformation, 104*, Article 102543. https://doi.org/10.1016/j.jag.2021.102543

Zhu, Y., Geiß, C., So, E., & Jin, Y. (2021c). Multitemporal relearning with convolutional LSTM models for land use classification. *IEEE Journal of Selected Topics in Applied Earth Observations and Remote Sensing, 14*, 3251–3265. https://doi.org/10.1109/JSTARS.2021.3055784

Zink, M., Moreira, A., Bachmann, M., Rizzoli, P., Fritz, T., Hajnsek, I., … Wessel, B. (2017). The global TanDEM-X DEM — A unique data set. In *2017 IEEE International Geoscience and Remote Sensing Symposium (IGARSS)* (pp. 906–909). https://doi.org/10.1109/IGARSS.2017.8127099